CrystEngComm

Accepted Manuscript

ROYAL SOCIETY OF CHEMISTRY

www.rsc.org/crystengcomm

CrystEngComm

ARTICLE

Pathway of Zinc Oxide Formation by Seed-Assisted and Controlled Double-Jet Precipitation

Received 00th January 20xx,
Accepted 00th January 20xx

DOI: 10.1039/x0xx00000x

www.rsc.org/

Xu Yan [a], Liyuan Chai [a,b], Qingzhu Li [a b,*], Lijun Ye [a], Bentao Yang [a], Qingwei Wang [a,b]

Zinc oxide formation in a seed-assisted and controlled double-jet precipitation (CDJP) was explored. Results show that the formation of ZnO involves the initial surface precipitation of β-$Zn(OH)_2$ intermediates on seed surfaces, followed by a fast surface phase transformation to ZnO. During this process, seeds play the role of crystallization catalyst to promote ZnO formation in a short time at room temperature via changing the precipitation pathway. Meanwhile, CDJP ensures the effects of seeds by controlling the solution supersaturation.

1 Introduction

Precipitation is a fundamental and ubiquitous process commonly used in water purification [1-3]. To enhance purification ability and precipitation rate, seed-assisted approach is preferred to adopt because of its simplicity and effectiveness [4, 5]. Most of the previous work focused on the influence of seed properties on the products morphology and ability [6, 7]. Some others studied the effect of seed addition on the removal efficiency of contaminants [8, 9]. In our recent studies [10, 11], a seed-assisted control double-jet precipitation (CDJP) was developed to produce abiological granular sludge (ABGS) during heavy metal wastewater treatment. This kind of sludge is confirmed to have excellent settling ability. The settling velocity of ABGS can reach up to > 4.0 cm/s, which is much higher than that of common sludge (< 1 cm/s). Although the effect of seed types and dosages was systematically investigated [11, 12], the detailed pathway of seed-assisted CDJP process and the role of seed playing in this process were not clarified.

Except adding seeds, solution supersaturation is also important for controlling precipitate formation. It is not practicable to control precipitation only by adding seed without regulating supersaturation [4]. When the degree of solution supersaturation is high, primary homogenous nucleation is always dominant even though seeds are added [13, 14]. For example, as reported by Mokone et al. [13], adding seed in a metal sulfide precipitation process has little effect on crystallization and sedimentation. This is because that the high solution supersaturation and primary homogenous nucleation prevalent during metal sulfide precipitation are difficult to control. For water purification, primary homogenous nucleation favors the production of small precipitates that are difficult to settle [12, 15]. Therefore, dewatering must be carried out by either filtration or centrifugation, which causes additional equipment and operational costs. To overcome these problems, CDJP is alternative and well applied [10, 11]. The main idea of CDJP is to keep a low solution supersaturation by controlling the reaction and stirring conditions during solution crystallization [16]. Initially, CDJP was used for photography to prepare silver halide particles with narrow size distribution, well-developed habit, precise internal composition, and epitaxy [17]. Currently, CDJP is one of the promising techniques for preparing many other particles, such as hydroxyapatite [18], ZnO [19, 20], CuO [21], and $Cu_2(OH)_3NO_3$ [22]. In addition, in other hydrothermal processes, the formation of well-growth metal oxide (e.g., ZnO and CuO) always needs a temperature as least 60~80 °C [23, 24]. Instead, CDJP can realize the formation of metal oxide at room temperature, but the reason is not well understood [19].

ZnO has been the subject of recent interest due to its potential applications in gas-sensing, photo detector, catalysis, dye-sensitized solar cells, sensors, and electronic materials [25-33], and thus is used as the target particle in this study. Herein, the pathway of ZnO formation in a seed-assisted CDJP was investigated using X-ray diffraction (XRD), X-ray photoelectron spectroscopy (XPS), scanning electron microscope (SEM), and transmission electron microscope (TEM). Role of seeds and CDJP playing in this process is determined.

2 Experimental section

2.1 Materials

Commercial ZnO seeds were purchased from Xilong Chemical Co.. And their XRD pattern is shown in Figure S1 in Supporting Information (SI). Zinc nitrate hexahydrate ($Zn(NO_3)_2 \cdot 6H_2O$) and sodium hydroxide (NaOH) were obtained from the Sinopharm Chemical Reagent Co., Ltd.. All chemicals used were of analytical grade and without further purification. Ultrapure water was used in the experiments.

[a] School of Metallurgy and Environment, Central South University, Changsha 410083, China
[b] Chinese National Engineering Research Centre for Control & Treatment of Heavy Metal Pollution, Changsha 410083, China
* Corresponding author at: School of Metallurgy and Environment, Central South University, 410083 Changsha, Hunan, China. Tel.: +86 731 88830875; fax: +86 731 88710171. E-mail address: qingzhuli@csu.edu.cn (Q. Li).
Electronic Supplementary Information (ESI) available:
See DOI: 10.1039/x0xx00000x

2.2 Precipitation Experiment

The procedure of CDJP was in accordance with that of previous studies [10, 11]. Typically, 100 mL ultrapure water containing 0.15 g ZnO seeds were induced into a 1000 mL reactor. Then, solution containing Zn(II) (1000 mg/L) was dropped in the reactor at the flow rate of 2.5 mL/min controlled by a peristaltic pump. The total injection time was adjusted to 60 min. The pH was kept at 9.0 ± 0.2 by dripping 0.015 M NaOH solution and was constantly monitored using a pH meter. Agitation of 500 rpm was designed to disperse the solution and particles by a magnetic stirrer in a temperature controlled water bath at 25 ± 1 °C. These reaction conditions have been previously optimized for the formation of ABGS with fast settling performance [10, 11]. Each experiment was carried out three times. Here, the samples withdrawn at 15, 30, and 60 min during seed-assisted CDJP were denoted as C15, C30, C60, respectively. After 60 min for injection, the mixture was stirred for additional 30 min (denoted as AC30). Precipitate samples were centrifuged, filtrated, washed using distilled water, and dried in a desiccant chamber at room temperature.

For comparison, seed-assisted experiment without applying CDJP, *i.e.*, NaOH solution was added to $Zn(NO_3)_2$ solution in a single step, was carried out as control. In detail, 150 mL $Zn(NO_3)_2$ solution (1000 mg/L) was added in 100 mL ultrapure water containing 0.15 g ZnO seeds. Then, NaOH solution (0.015 M) was added in a single step to adjust the solution pH to 9.0 ± 0.2. Other conditions are same with that in seed-assisted CDJP experiment. Samples collected at 15, 30, 60, and 90 min during control experiments were named as B15, B30, B60, and B90, respectively. Furthermore, CDJP experiments without adding seeds have been widely studied by others [19, 20]. Hence, these experiments were not performed in this study.

2.3 Characterizations

XRD pattern was recorded on a TTR III diffractometer (Rigaku Co., Japan) using Cu Kα radiation (λ=0.1542 nm). XPS measurement was carried out on an ESCALAB 250Xi spectrometer (Thermo Fisher Scientific, USA). Sample morphology and microstructure were examined using SEM (JSM-6360LV, Japan) and TEM (Tecnai G2, Czech Republic). SEM samples were coated with 2 nm of gold to enhance contrast.

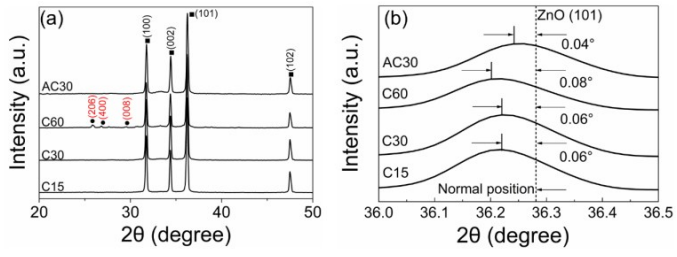

Figure 1 XRD patterns of seed-assisted CDJP samples (a) and enlarged ZnO (101) diffraction peaks (b)

3 Results

XRD patterns of precipitate samples are depicted in Figure 1. As shown in Figure 1a, all the samples show diffraction peaks at 2θ=31.7° (100), 34.4° (002), 36.2° (101), and 47.6° (102), indexing to hexagonal würtzite ZnO (PDF No. 36-1451) [24]. For C15 and C30, the intensity of these peaks slightly increases but no other peaks are observed. This phenomenon possibly implies oriented growth of new precipitates on ZnO seed surfaces at the early stage. As precipitation progresses, XRD peaks of β-$Zn(OH)_2$ (PDF No. 20-1435) were observed at 25.9° (206), 26.8° (400), and 29.6° (008) for C60. As known, this β-type of $Zn(OH)_2$ is a metastable-layered phase and an intermediate phase of ZnO [34]. For C15 and C30, no peak of β-$Zn(OH)_2$ was observed. This is possibly because the concentration of the new formed β-$Zn(OH)_2$ is too low to be detected by XRD at the initial stage. Also, this β-$Zn(OH)_2$ phase is not detected in AC30, which is likely the result of transformation of β-$Zn(OH)_2$ into ZnO with additional reaction. These speculations on β-$Zn(OH)_2$ formation and transformation will be further verified in the following sections.

Moreover, the (101) planes of ZnO show left shifts by careful observation (Figure 1b). The deviations for C15, C30, and C60 are 0.06°, 0.06°, and 0.08°, respectively, indicating a gradual increase in the lattice spacing of ZnO seeds with seed-assisted CDJP reaction progressing [35]. As known, two ways can cause lattice expansion. One is new precipitates occupies in the octahedral interstice of ZnO seeds. The other is ambient Zn^{2+} cations substitute O^{2-} ions in ZnO seeds, and hence the Coulomb force between Zn^{2+} cations expands the lattice [36]. Herein, lattice expansion indicates that new precipitate incorporates into ZnO lattice [37] and then promotes the oriented growth of new precipitates on seed surfaces. However, for AC30, the position of (101) peak shifts to the normal position with a smaller deviation of 0.04°. As mentioned above, this phenomenon is attributed to the transformation of β-$Zn(OH)_2$ to ZnO. Similar deviations are also observed in other diffraction peaks such as (100) and (002) peaks (Figure S2).

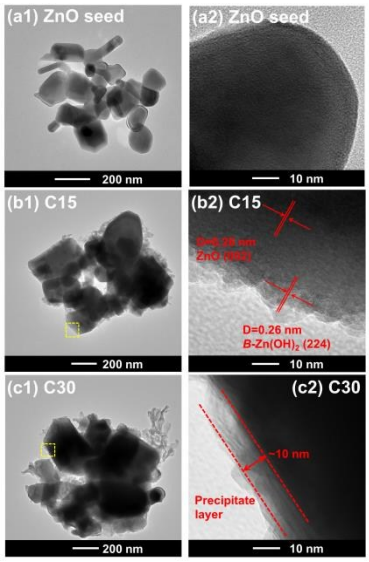

Figure 2 TEM and HRTEM images of ZnO seed (a1 and a2), C15 (b1 and b2), and C30 (c1 and c2)

The oriented growth behavior of β-$Zn(OH)_2$ on ZnO seed surfaces at the early stage can also be confirmed by TEM analysis (Figure 2). As shown, ZnO seeds have polygonal shapes with sharp edges. For C15, the sharp edges of ZnO seed become rough. For C30, these rough surfaces become precipitate layer with thickness of ~10 nm. Based on XRD results, the rough surface and precipitate layer result from the stacking of β-$Zn(OH)_2$ crystallites on seed surfaces. Moreover, the lattice spacing of ZnO seed and rough surface were determined as 0.26 nm, which is in good agreement with the (002) and (224) interplanar spacing of ZnO and β-$Zn(OH)_2$, respectively [38]. Besides, the (224) planes of β-$Zn(OH)_2$ parallel to the (002) ones of ZnO, forming β-$Zn(OH)_2$ (224) // ZnO (002). These phenomena further imply the oriented growth of β-$Zn(OH)_2$ on ZnO surfaces at the early stage of process [39].

XRD analysis is not suitable for analyzing amorphous and surface species, and thus XPS analysis was carried out. Figure 3 shows the high-resolution XPS spectra of Zn 2p 3/2. For all samples, the Zn 2p 3/2 peaks can be de-convoluted into two distinct peaks. The dominant peak at 1021.2 eV is associated with the Zn^{2+} in ZnO würtzite structure and the peak at 1022.3 eV is associated with $Zn(OH)_2$ species [40]. XPS results confirm the existence of $Zn(OH)_2$ species during seed-assisted CDJP process.

In addition, the surface content of ZnO and β-$Zn(OH)_2$ was estimated (Table 1). As listed, with CDJP reaction increasing to 60 min, the surface content of ZnO generally decreases to 64.1% while the surface content of β-$Zn(OH)_2$ increases to 35.9%. However, the bulk content of β-$Zn(OH)_2$ is too low to be calculated via XRD analysis. Recall that XPS is a surface selective analytical technique, while XRD is for bulk phase: the β-$Zn(OH)_2$ is determined on the surface [41]. This is powerful evidence for the oriented growth of β-$Zn(OH)_2$ on seed surfaces. As CDJP is stopped and additional reaction lasted for 30 min, the content of ZnO rises to 94% again, indicating the transformation of surface β-$Zn(OH)_2$ to ZnO.

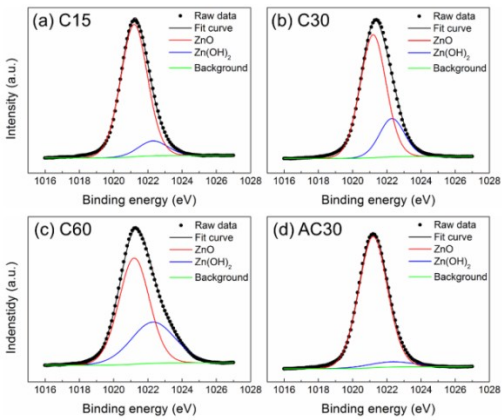

Figure 3 High-resolution of Zn 2p 3/2 XPS spectra of seed-assisted CDJP samples

Table 1 XPS Data of Zn 2p 3/2 spectra peaks

Species	Peak (eV)	Surface content, at. %			
		C15	C30	C60	AC30
ZnO	1021.2	89.1	76.7	64.1	94.0
$Zn(OH)_2$	1022.3	10.9	23.3	35.9	6.0

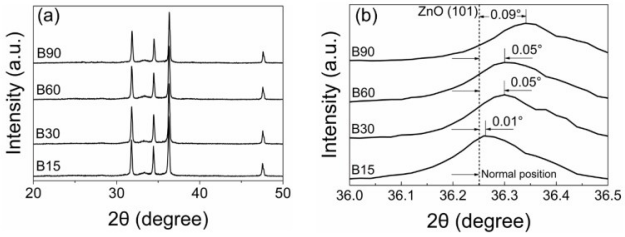

Figure 4 XRD patterns of control samples (a) and enlarged ZnO (101) diffraction peaks of samples (b)

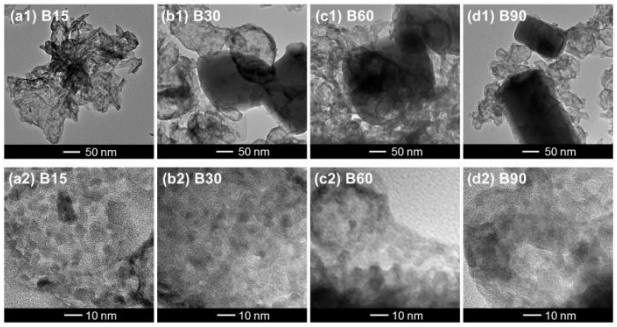

Figure 5 TEM images of control samples

For control experiment, the situations are far different from seed-assisted CDJP process. Specifically, XRD peaks (Figure 4a) of control samples become wider and lower than those of seed-assisted CDJP samples. This is a manifestation of higher lattice disorder in control samples. In addition, right shifts of (101) XRD peaks are detected (Figure 4b) for control samples, which are contrary to seed-assisted CDJP samples. The right shifts and broadening of XRD peaks both reflect the decrease in size of control samples [42, 43]. This further indicates that new precipitates in control samples are likely to be amorphous phase that always has a very small size. Moreover, the amorphous structure of new precipitates in control samples can be confirmed by the TEM (Figure 5) and SEM (Figure S3) observations. Figure 5 shows that the new precipitates are irregularly aggregate to form amorphous network structure. Figure S3 presents the SEM images of control samples obtained at different reaction time, where the full flocculent morphology is clearly observed. Furthermore, XPS analysis demonstrates that the surface content of $Zn(OH)_2$ in all control samples is estimated as 17±1% (Figure 6 and Table 2), indicating that the mechanism of control precipitation is independent of seed surfaces.

4. Discussion

Based on above analysis, we conclude that the formation of ZnO in seed-assisted CDJP involves the oriented growth of β-$Zn(OH)_2$ intermediates on seed surfaces at the initial stages, followed by a surface phase transformation from β-$Zn(OH)_2$ to ZnO (Figure 7). During this process, ZnO seed indeed plays its role as seeding materials as observed by TEM images (Figure 2). At the same time, the application of CDJP ensures its function. Without applying CDJP, the extremely high supersaturation in the solution is difficult to control and the addition of seeds will make no sense to the precipitation, as confirmed by the XRD, TEM, and XPS results of control experiments.

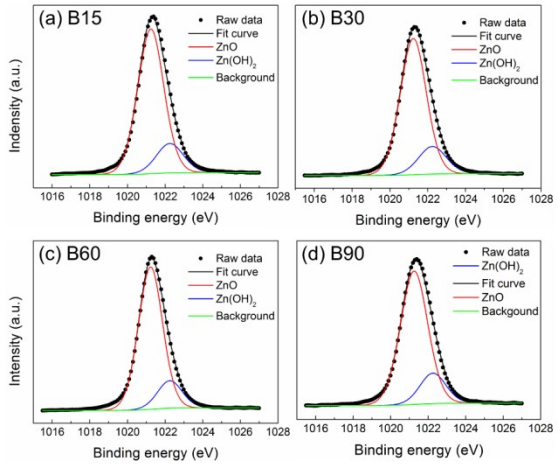

Figure 6 High-resolution of Zn 2p 3/2 XPS spectra of control samples

Table 2 XPS Data of Zn 2p 3/2 spectra peaks of control samples

Species	Peak (eV)	Surface content, at. %			
		B15	B30	B60	B90
ZnO	1021.2	82.5	82.3	83.4	82.2
$Zn(OH)_2$	1022.3	17.5	17.7	16.6	17.8

It is also worth noting that, the added seeds not only function as seeding materials, but also play a catalysis effect on the formation of ZnO. Generally, the formation of ZnO in zinc-bearing alkaline solution always needs a high reaction temperature (at least 60~80 °C) [23, 24]. Although CDJP can reduce this temperature to room temperature, the reaction time for ZnO formation in CDJP without adding seeds always needs as least 2 h [19, 20]. However, as indicated by the XPS results (Figure 3 and Table 1), the transformation of surface β-$Zn(OH)_2$ to ZnO is nearly achieved in a much shorter time (~30 min) at room temperature in seed-assisted CDJP. Such fast reaction is mainly owing to the change of ZnO formation pathway catalyzed by seed as described in Figure 7. For confirmation, the thermodynamic data of related species and reactions are listed in Table S1 and S2 [44]. Also, reference XRD patterns of ZnO, ε-$Zn(OH)_2$, and β-$Zn(OH)_2$ are presented in Figure S4.

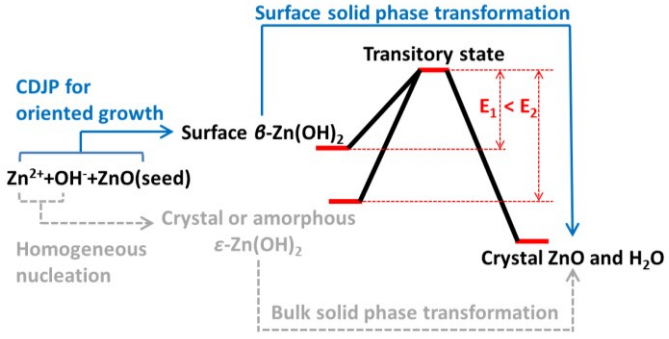

Figure 7 Schematic diagram of ZnO formation mechanism in different process

In zinc-bearing alkaline solution (pH~9), the intermediate for the ZnO formation is always crystal or amorphous ε-$Zn(OH)_2$ [20, 24, 45]. This ε-$Zn(OH)_2$ is thermodynamically metastable with respect to ZnO (ΔG^o_r = -2.53 kJ/mol). Although this value of ΔG^o_r is an indication of a spontaneous reaction, the rate of transition from ε-$Zn(OH)_2$ to ZnO is extremely slow at room temperature. As reported, solid zinc hydroxide remains unchanged after six months in water at room temperature [46]. That is, the transformation from ε-$Zn(OH)_2$ to ZnO at room temperature is kinetically stable and needs overcome a high activation energy barrier (E_2 in Figure 7).

For comparison, the intermediate is changed to β-$Zn(OH)_2$ in seed-assisted CDJP. As seen in Figure S4, the (002) plane of ZnO is highly consistent with the (224) plane of β-$Zn(OH)_2$. This provides the condition for the oriented growth of β-$Zn(OH)_2$ on ZnO seed surface. Indeed, the oriented growth of (224) plane of β-$Zn(OH)_2$ on (002) plane of ZnO is observed in the TEM image (Figure 2d). This surface β-$Zn(OH)_2$ is more thermodynamically unstable with respect to ZnO with ΔG^o_r = -4.49 kJ/mol, which is lower than that of ε-$Zn(OH)_2$. More importantly, in view of kinetics, seeding materials can lower the activation energy barrier (E_1 in Figure 7) of surface transformation. As it is well known, the creation of a new free crystal surface is much more difficult than creation of an interface between the new crystallites and seed. Here, ZnO seeds provide a large amount of pre-existing interfaces. Little energy for creating new ZnO free surfaces is needed. It is therefore reasonable to suspect that the activation energy barrier in seed-assisted CDJP will be greatly lowered [47, 48]. As a conclusion, seed-assisted CDJP has the advantages to promote ZnO formation in a short time at room temperature in view of both thermodynamics and kinetics. Mihaela Jitianu and Dan V. Goia [20] previously speculated that the facile and fast formation of ZnO possibly attributed to the formation of some more reactive form of zinc hydroxide. Here, we reveal that this more reactive form of zinc hydroxide is surface β-$Zn(OH)_2$.

Conclusion

In this study, the pathway of ZnO formation in seed-assisted CDJP was determined. Results demonstrated that the pathway involves the initial oriented growth of metastable-layered β-$Zn(OH)_2$ intermediates on seed surfaces, followed by a fast surface phase transformation to ZnO. It is noteworthy that, seeds play a role of crystallization catalyst to realize the formation of ZnO in such short time at room temperature. As a rapid, facile and effective way to form ZnO, this seed-assisted CDJP process is desirable for heavy metal wastewater treatment, as well as other applications related to precipitation.

Acknowledgements

This work was supported by National Natural Science Foundation of China (51504299); Science and Technology Program for Public Wellbeing (2012GS430201); The Key Project of Science and Technology of Hunan Province, China (2012FJ1010) for financial support.

Notes and references

1. T. Wang, L. Zhang, C. Li, W. Yang, T. Song, C. Tang, Y. Meng, S. Dai, H. Wang, L. Chai and J. Luo, *Environ. Sci. Technol.*, 2015, **49**, 5654-5662.
2. M. Tong, S. Yuan, P. Zhang, P. Liao, A. N. Alshawabkeh, X. Xie and Y. Wang, *Environ. Sci. Technol.*, 2014, **48**, 5145-5153.
3. Y. Jia, D. Zhang, R. Pan, L. Xu and G. P. Demopoulos, *Water Res.*, 2012, **46**, 500-508.
4. N. Karapinar, E. Hoffmann and H. H. Hahn, *Water Res.*, 2004, **38**, 3059-3066.
5. Z. Liu, Q. Zhao, L. Wei, D. Wu and L. Ma, *J. Chem. Technol. Biot.*, 2011, **86**, 1394-1398.
6. Y. Deng, J. Zhao, Q. Li, X. Xu, H. Lin and Y. Li, *CrystEngComm*, 2014, **16**, 5184-5188.
7. T. Kawano and H. Imai, *Colloid Surf. A*, 2008, **319**, 130-135.
8. S. J. Coles and T. L. Threlfall, *CrystEngComm*, 2014, **16**, 4355-4364.
9. C. Su, L. D. Dulfo, M. L. P. Dalida and M. Lu, *Sep. Purif. Technol.*, 2014, **125**, 90-96.
10. X. Yan, Q. Li, L. Chai, B. Yang and Q. Wang, *Chemosphere*, 2014, **113**, 36-41.
11. L. Chai, X. Yan, Q. Li, B. Yang and Q. Wang, *Environ. Sci. Pollut. R.*, 2014, **21**, 12436-12444.
12. X. Yan, L. Chai and Q. Li, *Sep. Sci. Technol.*, 2013, **48**, 1442-1449.
13. T. P. Mokone, R. P. van Hille and A. E. Lewis, *Water Res.*, 2012, **46**, 2088-2100.
14. T. P. Mokone, R. P. van Hille and A. E. Lewis, *J. Colloid Interf. Sci.*, 2010, **351**, 10-18.
15. D. K. Villa-Gomez, E. D. van Hullebusch, R. Maestro, F. Farges, S. Nikitenko, H. Kramer, G. Gonzalez-Gil and P. N. L. Lens, *Environ. Sci. Technol.*, 2014, **48**, 664-673.
16. J. Stavek, M. Sipek, I. Hirasawa and K. Toyokura, *Chem. Mater.*, 1992, **4**, 545-555.
17. Q. Zhong and E. Matijevi C, *J. Mater. Chem.*, 1996, **6**, 443-447.
18. S. Sánchez-Salcedo, M. Colilla, I. Izquierdo-Barba, M. Vallet-Reg íand M. Abbo, *J. Mater. Chem. B*, 2013, **1**, 1595-1606.
19. A. P. A. Oliveira, J. Hochepied, F. Grillon and M. Berger, *Chem. Mater.*, 2003, **15**, 3202-3207.
20. M. Jitianu and D. V. Goia, *J. Colloid Interf. Sci.*, 2007, **309**, 78-85.
21. S. Lee, Y. Her and E. Matijević, *J. Colloid Interf. Sci.*, 1997, **186**, 193-202.
22. C. Henrist, K. Traina, C. Hubert, G. Toussaint, A. Rulmont and R. Cloots, *J. Cryst. Growth*, 2003, **254**, 176-187.
23. M. Wang, Y. Zhang, Y. Zhou, F. Yang, E. J. Kim, S. H. Hahn and S. G. Seong, *CrystEngComm*, 2012, **15**, 754-763.
24. J. Wang, S. Hou, L. Zhang, J. Chen and L. Xiang, *CrystEngComm*, 2014, **16**, 7115-7123.
25. Y. Cai, X. Li, Y. Liu, S. Du, P. Cheng, F. Liu, K. Shimanoe, N. Yamazoe and G. Lu, *CrystEngComm*, 2014, **16**, 6135-6140.
26. W. Zang, P. Li, Y. Fu, L. Xing and X. Xue, *RSC Adv.*, 2015, **5**, 84343-84349.
27. M. Chen, L. Hu, J. Xu, M. Liao, L. Wu and X. Fang, *Small*, 2011, **7**, 2449-2453.
28. V. Q. Dang, T. Q. Trung, D. Kim, L. T. Duy, B. Hwang, D. Lee, B. Kim, L. D. Toan and N. Lee, *Small*, 2015, **11**, 3054-3065.
29. B. Zhao, F. Wang, H. Chen, Y. Wang, M. Jiang, X. Fang and D. Zhao, *Nano Lett.*, 2015, **15**, 3988-3993.
30. L. Chai, X. Yan, Q. Li, B. Yang, X. Wang and Q. Wang, *Sep. Purif. Technol.*, 2015, **151**, 66-73.
31. L. Hu, J. Yan, M. Liao, H. Xiang, X. Gong, L. Zhang and X. Fang, *Adv. Mater.*, 2012, **24**, 2305-2309.
32. X. Fang, Y. Bando, U. K. Gautam, T. Zhai, H. Zeng, X. Xu, M. Liao and D. Golberg, *Crit. Rev. Sold State Mater. Sci.*, 2009, **34**, 190-223.
33. C. Hsu and S. Chang, *Small*, 2014, **10**, 22.
34. F. Demoisson, R. Piolet and F. Bernard, *Cryst. Growth Des.*, 2014, **14**, 5388-5396.
35. A. Khataee, R. Darvishi Cheshmeh Soltani, Y. Hanifehpour, M. Safarpour, H. Gholipour Ranjbar and S. W. Joo, *Ind. Eng. Chem. Res.*, 2014, **53**, 1924-1932.
36. X. G. Xu, H. L. Yang, Y. Wu, D. L. Zhang, S. Z. Wu, J. Miao, Y. Jiang, X. B. Qin, X. Z. Cao and B. Y. Wang, *Appl. Phys. Lett.*, 2010, **97**, 232502.
37. Z. Wu, W. Huang, K. Cui, Z. Gao and P. Wang, *J. Hazard. Mater.*, 2014, **278**, 91-99.
38. P. Li, H. Liu, B. Lu and Y. Wei, *J. Phy. Chem. C*, 2010, **114**, 21132-21137.
39. M. Huang, Y. Yan, W. Feng, S. Weng, Z. Zheng, X. Fu and P. Liu, *Cryst. Growth Des.*, 2014, **14**, 2179-2186.
40. S. Sepulveda-Guzman, B. Reeja-Jayan, E. de la Rosa, A. Torres-Castro, V. Gonzalez-Gonzalez and M. Jose-Yacaman, *Mater. Chem. Phys.*, 2009, **115**, 172-178.
41. N. J. Nicholas, G. V. Franks and W. A. Ducker, *CrystEngComm*, 2012, **14**, 1232-1240.
42. K. M. Reddy, S. V. Manorama and A. R. Reddy, *Mater. Chem. Phys.*, 2003, **78**, 239-245.
43. S. Hao, X. Zhang, X. Mei, T. Grosdidier and C. Dong, *Mater. Lett.*, 2008, **62**, 414-417.
44. J. A. Dean, *Lange's Handbook of Chemistry*, McGraw-Hill, New York, 1979.
45. M. Wang, Y. Zhou, Y. Zhang, S. H. Hahn and E. J. Kim, *CrystEngComm*, 2011, **13**, 6024-6026.
46. A. Moezzi, M. Cortie and A. McDonagh, *Dalton T.*, 2011, **40**, 4871-4878.
47. G. Z. Papageorgiou, D. S. Achilias, D. N. Bikiaris and G. P. Karayannidis, *Thermochim. Acta.*, 2005, **427**, 117-128.
48. J. F. Banfield, S. A. Welch, H. Z. Zhang, T. T. Ebert and R. L. Penn, *Science*, 2000, **289**, 751-754.

ZnO can be well formed in a short time at room temperature via a seed-assisted and controlled double-jet precipitation.